University of Baghdad
College of Engineering
JE
JOURNAL OF ENGINEERING

Journal of Engineering
journal homepage: www.joe.uobaghdad.edu.iq
Number 2 Volume 28 February 2022

Civil and Architectural Engineering

Nonlinear Finite Element Analysis of Fiber Reinforced Concrete Pavement under Dynamic Loading

Hadeel M. Shakir
Researcher College of Engineering, Al-Nahrain University
Baghdad, Iraq
hadeelmahmood123@gmail.com

Adel A. Al-Azzawi
Prof, College of Engineering, Al-Nahrain University,
Baghdad, Iraq
Dr_adel_azzawi@yahoo.com

Ahmed Farhan Al-Tameemi
Lecturer, College of Engineering, Al-Nahrain University,
Baghdad, Iraq
ahmed.f.altameemi@ced.nahrainuniv.edu.iq

ABSTRACT

The analysis of rigid pavements is a complex mission for many reasons. First, the loading conditions include the repetition of parts of the applied loads (cyclic loads), which produce fatigue in the pavement materials. Additionally, the climatic conditions reveal an important role in the performance of the pavement since the expansion or contraction induced by temperature differences may significantly change the supporting conditions of the pavement. There is an extra difficulty because the pavement structure is made of completely different materials, such as concrete, steel, and soil, with problems related to their interfaces like contact or friction. Because of the problem's difficulty, the finite element simulation is the best technique incorporated in the analysis of rigid pavements. The ABAQUS software was used to conduct the response of previously tested specimens under different loading conditions. Good agreement between the laboratory and finite element results was observed. The maximum differences between experimental and finite element outcomes in terms of ultimate loads and ultimate deflection for rigid pavements under monotonic loading are 6% and 8%, respectively, and 10% and 18% respectively for the repeated load.

Keywords: rigid pavements, fiber concrete, finite element

تحليل العناصر المحدودة غير الخطية للتبليط الخرساني المسلح المقوى بالألياف تحت التحميل الديناميكي

هديل محمود شاكر
باحث
كلية الهندسة جامعة النهرين

د.عادل عبد الامير العزاوي
استاذ
كلية الهندسة جامعة النهرين

د. احمد فرحان التميمي
مدرس
كلية الهندسة جامعة النهرين

الخلاصة

يعتبر تحليل الأرصفة الصلبة مهمة معقدة لأسباب عديدة. أولاً ، تشمل ظروف التحميل تكرار أجزاء من الأحمال المطبقة (الأحمال الدورية) ، والتي تؤدي إلى إجهاد مواد الرصف. بالإضافة إلى ذلك ، تكشف الظروف المناخية عن دور مهم في أداء الرصيف حيث أن التمدد أو الانكماش الناجم عن اختلاف درجات الحرارة قد يغير بشكل كبير الظروف الداعمة للرصيف. هناك صعوبة

*Corresponding author
Peer review under the responsibility of University of Baghdad.
https://doi.org/10.31026/j.eng.2022.02.06

Article received: 16/5/2021
Article accepted:27/6/ 2021
Article published:1/2/2022

إضافية لأن هيكل الرصيف مصنوع من مواد مختلفة تمامًا ، مثل الخرسانة والصلب والتربة ، مع وجود مشاكل متعلقة بالواجهات مثل التلامس أو الاحتكاك. نظرًا لصعوبة المشكلة ، فإن محاكاة العناصر المحدودة هي أفضل تقنية مدمجة في تحليل الأرصفة الصلبة. تم استخدام برنامج ABAQUS لإجراء استجابة العينات التي تم اختبارها مسبقًا في ظل ظروف تحميل مختلفة. تمت ملاحظة توافق جيد بين المختبر ونتائج العناصر المحدودة. كانت الفروق القصوى بين نتائج العناصر التجريبية والمحدودة من حيث الأحمال النهائية والانحراف النهائي للأرصفة الصلبة تحت التحميل الرتيب 6٪ و 8٪ على التوالي و 10٪ و 18٪ على التوالي للحمل المتكرر.

الكلمات الرئيسية: أرصفة صلبة ، خرسانة ليفية ، عنصر محدود

1. INTRODUCTION

The behavior of the rigid pavement is growing, and the need for carrying more analysis for improving the properties of concrete becomes larger. The weakness of tensile strength due to hard conditions is one of the orientations in previous research. The development or improvement of the concrete in rigid pavement by using the fibers is an important issue. These fibers, which spread in concrete, will usually improve material properties such as flexural strength, energy absorbed, ductility, toughness, fatigue strength, impact resistance, and accompanied with a slight enhancement in compressive strength **(Daniel et al., 2002)**. The most important characteristic of any method of analyzing rigid concrete pavement is the performance, precision, and solution economy. One of the effective methods utilized for investigating members' responses is the finite element simulation. This technique is a numerical method used to simulate stresses and deformation and to analyze various geometry members. The rigid pavement is discretized into smaller manageable finite elements with nodes that are used to define deformations and connect each element to the other. The accuracy of the results obtained by using such a technique is influenced by the arrangement, form, and a variety of other factors affecting the body mesh. Since the 1960s, the FEM has grown to be one of the tremendous techniques used to simulate engineering problems and the most useful research methods. The simulation by FEM reveals the capability to effectively model concrete pavement under various loads **(Ergatoudis, Irons, and Zienkiewicz, 1968).** This study employs ABAQUS 6.12 software which compromises a set of powerful engineering simulation subroutines used to model various complicated geometry and loading problems with linear and nonlinear responses. ABAQUS increases the load increments automatically, and convergence tolerances then correct them continuously during nonlinear analysis to ensure accuracy and efficiency in solving problems **(ABAQUS 2012)**.

The numerical simulation of FRC has been given more consideration in recent years**. (Belletti and Cerioni, 2004)** presented experimental and numerical studies on the response of slabs made with fiber-reinforced concrete resting on grade for industrial pavements. This is done by testing four FRC slabs with fibers having various volume fractions and aspect ratios in the laboratory. The slabs must be placed on several steel springs to produce a Winkler subgrade. The finite element method uses to make numerical simulations based on nonlinear fracture mechanics. This extension concerns using a more realistic law for modeling the stiffness and strength of FRC after cracking the concrete matrix. Therefore, the model added the stiffness matrix for FRC with primary and secondary cracks. Finally, the findings of the experimental and finite element techniques were found to agree well, which provides valuable knowledge for design considerations. **(Khan and Harwalkar, 2014)** simulated the concrete pavements by using ANSYS software. The model of the concrete slab in FE is a solid 45 brick element, and the soil is spring elements. The analysis was carried out for a slab soil combination and a wide range of loads. Elastic springs reflect the soil such as "Winkler type". The soil stiffness was obtained from the sub-grade reaction module.

The main contribution of this study is to compare the model's stress results by using the method of finite elements with the classical approach of the method of Westergaard and IRC 58-2002. Compared to those obtained from ANSYS, Westergaard's equation under approximate edge wheel load stresses is validated. The bending laboratory test of steel fiber reinforced concrete specimens was simulated by **(Zimmer et al., 2015)** using the computer program 'ABAQUS'. The numerical 3D model of a three-point bending test using the testing machine under static loads up to its ultimate value is utilized. The loading rates were (0.5 and 1) kN/sec. The (SFRC) flexural members or beam specimens contain (0.0, 0.4, and 0.8%) steel fibers. Stress, strain, and deformation were obtained, and the "ABAQUS" simulation of the test was used. Results demonstrate that the magnitudes of deflection, stress, and strain are directly proportional to the increase in steel fiber and that the experimental results and the analytical methods can be fairly accepted. Finally, using 'ABAQUS,' a comparison of horizontal tensile stress and strain at the bottom of the concrete pavement with (0.0, 0.4, and 0.8) % steel fiber is made. The outcomes showed that the concrete pavement's ability to withstand higher magnitudes of tensile stress and strain without deterioration increases as the steel fiber content increases due to the increase in tensile stress.

2. FINITE ELEMENT MODELING

Nonlinear behavior modeling involved testing 12 square concrete pavements with a side length of 1000 mm and thickness of 120 mm. Tested concrete pavement is designed in accordance with ACI 318-19. Various parameters are considered in this study: steel reinforcement existing, fiber type (steel, glass, and hybrid), fiber content (V_f), and load nature (monotonic and repeated). In which the symbol N designates non-fibrous concrete, SF designates steel fiber concrete, GF designates glass fiber concrete, HF designates hybrid fiber concrete. The symbol RC designates reinforced concrete and symbol C designates plain concrete. The symbol P designates pavement and 1 is used for monotonic loading while 2 is used for repeated loading. **Table 1** shows the notation for the rigid pavement present study specimens. **Fig.1** illustrates the sample geometry and details of reinforcement.

Table 1. Description of specimens.

Mix type	Pavement No.	Notation of specimen	Description
A	P1	NRCP 1	Nonfibrous Reinforced Concrete Pavement with (0.0) % fibers content and subjected to Monotonic loading
	P2	NRCP 2	Nonfibrous Reinforced Concrete Pavement with (0.0) % fibers content and subjected to Repeated loading
B	P3	SFRCP 1	Steel Fiber Reinforced Concrete Pavement with (0.5) % steel fiber content and subjected to Monotonic loading

	P4	SFRCP 2	Steel Fiber Reinforced Concrete Pavement with (0.5) % steel fiber content and subjected to Repeated loading
C	P7	HFRCP 1	Hybrid Fiber Reinforced Concrete Pavement (0.25 +0.25) % steel and glass fiber contents and subjected to Monotonic loading
	P8	HFRCP 2	Hybrid Fiber Reinforced Concrete Pavement (0.25 +0.25) % steel and glass fiber contents and subjected to Repeated loading
	P9	HFCP 1	Hybrid Fiber Concrete Pavement (0.25 +0.25) % steel and glass fiber contents and subjected to Monotonic loading
	P10	HFCP 2	Hybrid Fiber Concrete Pavement (0.25 +0.25) % steel and glass fiber contents and subjected to Repeated loading

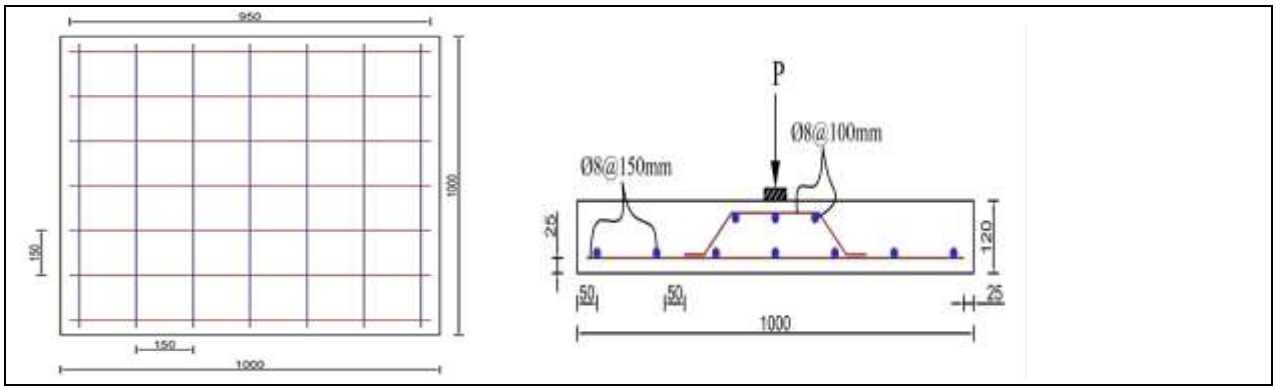

Figure 1. Reinforcement detail.

3. TYPE OF ELEMENT AND MESHING

To achieve high efficiency and retain precision, the suitable elements that are expected to represent the response are selected. Also, the appropriate material modeling that represents the fibrous and nonfibrous concrete is utilized **(Kwak and Filippou, 1990)**. The 3D eight-node linear brick element was used in the present study with minimized integration, and hourglass control (C3D8R) is shown in **Fig.2**. On the other hand, the steel reinforcement bar was modeled using the two-node linear three-dimensional truss element (T3D2) is shown in **Fig.3**. While the finite element mesh of the specimens with an element mesh size of 50 mm for concrete and rigid steel support and 25 mm for reinforcement bar and loaded plate.

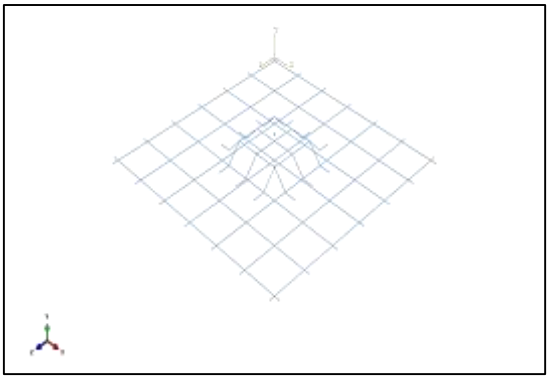

Figure 2. modeling of concrete pavement.

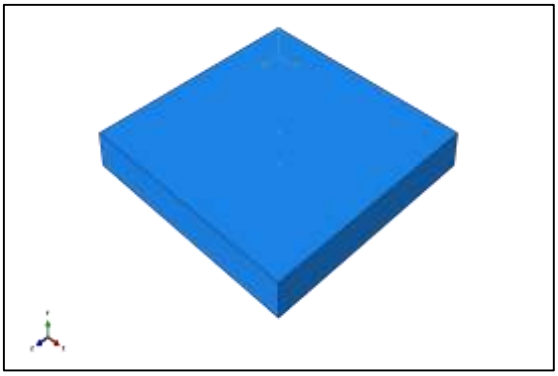

Figure 3. Reinforcement detail.

4. PROPERTIES OF MATERIALS

4.1 Concrete

The response of concrete pavements subjected to various stress components depends on different model methods, some of which model based on elasticity and some on plasticity. In ABAQUS, there are three approaches to model and analyze concrete material:

1- Standard material comprises damaged plasticity.
2- Standard material comprises smeared cracking.
3- Explicit concrete cracking model.

In this study, the damage plasticity approach can be used to model all forms of reinforced and unreinforced concrete members and other materials like soils with quasi-brittle behavior. Because of its ability to predict test output up to failure, this approach can be used to evaluate members subjected to monotonic, dynamic, and cyclic loading. **(ABAQUS, 2012)**. The modeling of fibers in concrete using the FE-code ABAQUS/CAE demonstrates that the program can simulate the actual fibrous concrete response with acceptable accuracy by treating it as a single part with concrete and using the damage plasticity simulation and the outcomes depend on the material characteristics (uniaxial compression and tension response of tested material). The compression stress-strain response is obtained from the equations tabulated in the BSI code. In addition to the modulus of elasticity and the Poisons ratio, the following parameters must be specified in the ABAQUS program:

1. At a high confining strain, the dilation angle ψ is determined in the p-q plane. It specifies the volume adjustment to the shear strain ratio. Most published research uses a dilation angle of 12^o to 37^o for concrete **(ABAQUS, 2012)** and **(Lundqvist, 2007)**.
2. When the Drucker-Prager function reaches the asymptote, ϵ is the rate, the plastic stream tends to a straight line as the eccentricity approaches zero. An eccentricity of 0.1 is used in subsequent calculations.
3. The default value of 1.16 for σ_{b0} /σ_{c0} (the initial biaxial compressive yield stress ratio to the initial uniaxial compressive yield stress) is selected.
4. μ is a viscosity parameter that shows the time it takes for the viscoplastic system to relax. This will improve the pavement specimen's numerical convergence during the softening process. Since the pavement model did not trigger significant convergence issues, the viscosity parameter should be set to zero.

5. K_c is the ratio of the second stress invariant on the tensile meridian to the compressive meridian at initial yield, with a used default value of 2/3.
These parameters are default data can be seen in **Table 2**. The concrete specimens are tested in the Laboratory of Civil Engineering Department of College of Engineering/Al- Nahrain University, and the properties of concrete are given in **Table 3.**

Table 2. Parameters of concrete damage plasticity for NRCP, SFRCP, HFRCP, and HFRCP 1%.

Poissons's ratio for concrete	0.2
Dilation angle	36
Eccentricity	0.1
f_{bo}/f_{co}	1.16
K_c	0.667
Viscosity parameter	0

Table 3. Mechanical properties of concrete for modeling.

Specimens	Compressive strength MPa	Splitting tensile strength MPa	Modulus of elasticity MPa
NRCP	32.50	3.226	26900.43
SFRCP	35.13	3.823	28877.53
HFRCP	38.27	3.795	28487.36
HFRCP 1%	42.10	3.940	30495.72

4.2 Steel Modeling

The steel reinforcement was modeled using the classic elastic-perfectly plastic model. This model is applied in ABAQUS and only needs the modulus of elasticity, Poisons ratio, yield stress and the corresponding strain obtained from the experimental work to be input in the software, as shown in **Table 4**. The steel plates under the load and the pavement were modeled as an elastic material. Only the modulus of elasticity and Poisons ratio is needed, as no failure in the steel plates is expected to simplify the analysis.

Table 4. Properties of steel bar reinforcement.

Steel bar	Stress MPa	Strain	Modulus of Elasticity MPa	Poissons's ratio
Rebar 8 mm	420	0	200000	0.3
	500	0.15		

4.3 Interaction

This property is used to connect various parts together to make them work as one component. **Table 5.** and **Fig.4.** given a different type of connection between sections.

Table 5. Type of connection between sections.

No.	Type of Contact	Type of Constrain	Used of Constrain
1	Embedded Region	Make contact between reinforcement and concrete	It is used to model embedded elements inside the host element and constrain translation.
2	Tie	- Make contact between the concrete surface and circular plate - Make contact between the concrete surface and rigid steel supports	It is used to bond the two surfaces together to make the translation constrain, and the two surfaces have the same degree of freedom.

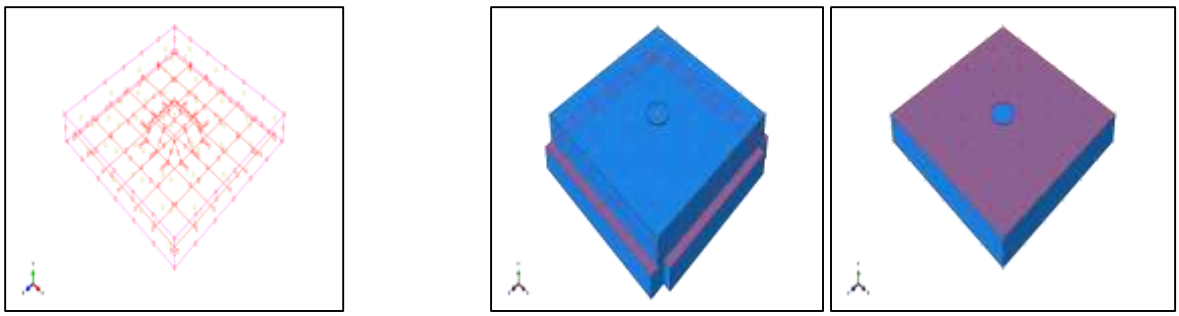

Figure 4. Interaction type reinforcement bar with concrete, circular plate with concrete, rigid steel support with concrete.

4.4 Boundary Condition and Limitations

The edge restrictions must be identified to constrain the pavement to get a unique solution. The boundary conditions are applied at points where the supports exist. This boundary condition was modeled as simply supported along four edges at the lower sides, as shown in **Fig.5**. Nodes at the bottom face prevented movement against y-direction for all sides according to their coordinates.

4.5 Loads

The type of loading analysis must be precisely defined in the step module after the assembly of the specimen parts. The static load on the pavement is identified using the option (static, general) in the program. A displacement value was applied above the circular plate specimens at the center of the concrete pavement, as shown in **Fig.6**. For the case of repeated loading, the loading was subjected to the selected specimens based on the loading protocol suggested by FEMA 461 **AGENCY, F. E. M. (2007)**.

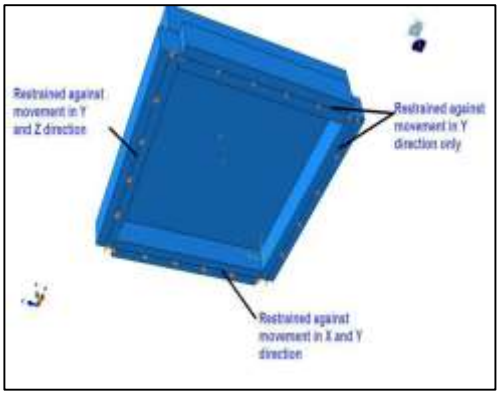

Figure 5. Pavement boundary conditions.

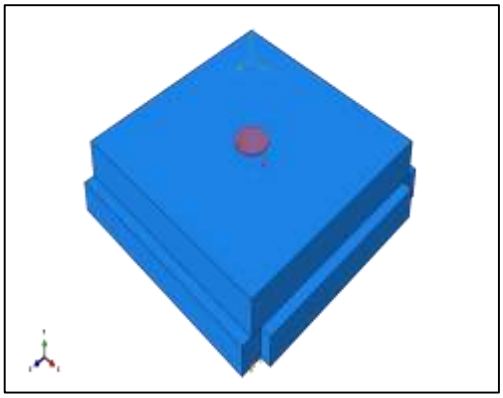

Figure 6. Concrete pavements under loads.

5. NUMERICAL ANALYSIS RESULTS

5.1 Load-deflection relationships

The numerical outcomes show a fair match with the experimental findings by **(Shakir, H., 2021).** The maximum differences between experimental and finite element outcomes in terms of ultimate loads and ultimate deflection for rigid pavements under monotonic loading are 6% and 8%, respectively. The model can predict the values with great accuracy, as shown in **Table 6. Figs.7 to 9** displays the centrally applied load variation with central deflections.

Table 6. Experimental and finite element analysis results of pavements subjected to monotonic load.

Pavement specimens	**Exp. Results**		**FEA. Results**		**P_u EXP. /P_u FEA.**	**Δ_u EXP./Δ_u FEA**
	P_u (kN)	Δ_u (mm)	P_u (kN)	Δ_u (mm)		
NRCP1	125.80	14	133.51	13.91	0.94	1.01
SFRCP1	151.40	16.76	158.16	15.40	0.95	1.08
HFRCP1	148.61	16.76	149.98	15.62	0.98	1.07

For repeated loading, the maximum differences between experimental and finite element outcomes in terms of ultimate loads and ultimate deflection for rigid pavements are 10% and 18%, respectively. The model can predict the values with lower accuracy for repeated loading, as shown in **Table 7**.

Table 7. Experimental and finite element analysis results of pavements subjected to repeated load.

Pavement specimens	Exp. Results		FEA. Results		P_u EXP. /P_u FEA.	Δ_u EXP./Δ_u FEA
	P_u (kN)	Δ_u (mm)	P_u (kN)	Δ_u (mm)		
NRCP2	107.72	11.50	119.12	11.21	0.90	1.02
SFRCP2	130.12	15.29	145.6	12.91	0.90	1.18
HFRCP2	142.92	16.10	145.88	13.86	0.97	1.16

The load-deformation curve obtained from the numerical simulation showed stiffer behavior compared to the experimental one. This is because micro-cracks caused by drying shrinkage and handling, which are present in the concrete to some extent, will reduce the stiffness of the actual specimens, while finite element models do not account for the micro-cracks. Also, some material parameters are assumed and not measured in the laboratory in finite elements. The program's repeated loading simulation has failed to trace the real behavior for some samples accurately.

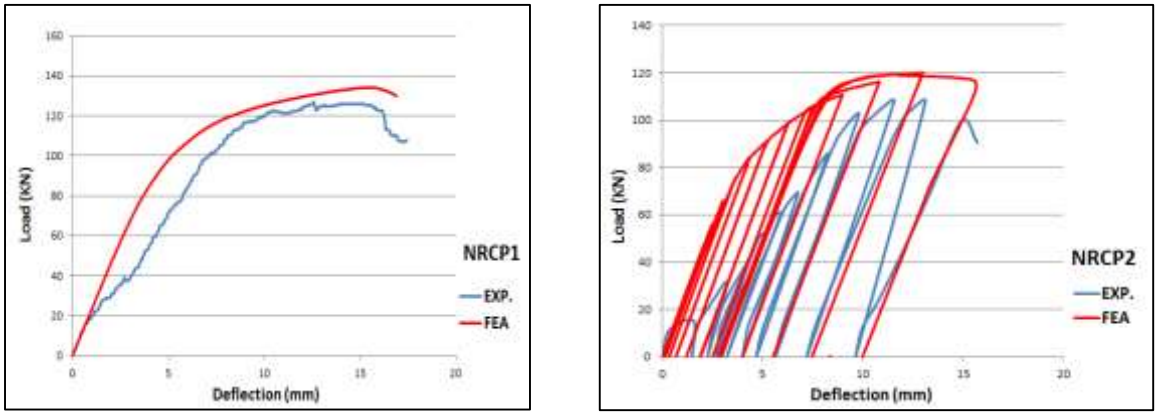

Figure 7. FEA and experimental load-deflection curves for specimen NRCP1 and NRCP2 under monotonic and repeated load.

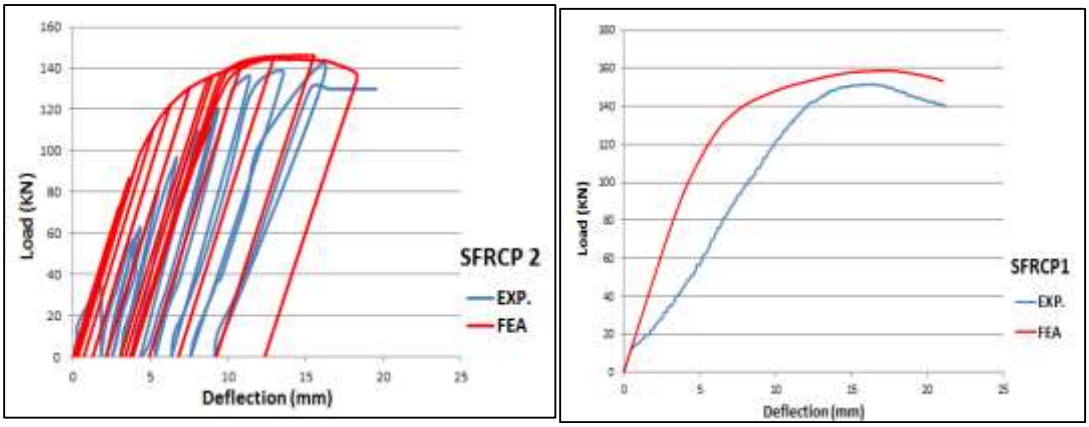

Figure 8. FEA and experimental load-deflection curves for specimen SFRCP1 and SFRCP2 under monotonic and repeated Load.

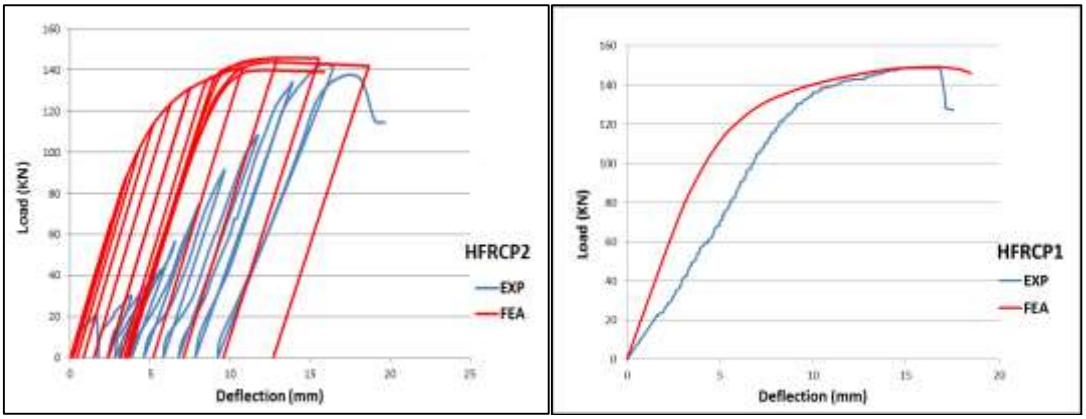

Figure 9. FEA and experimental load-deflection curves for specimen HFRCP1 and HFRCP2 under monotonic and repeated Load.

5.2 Crack Patterns Development

When the pavement fails, the cracking pattern on the stress side of the pavement spreads within the pavement adjacent to the center. The cracks propagate tangentially near the center with increasing load and then spread radially. The cracks are thought to be perpendicular to the maximum principal plastic strains, allowing the cracking direction to be seen through the maximum principal plastic strains. When the maximum principal plastic strain is positive, the concrete weakened or damaged plasticity model assumes cracking begins**. Figs. 10 - 15** compares the concrete crack patterns obtained from the FEA findings with those found in the experimental test.

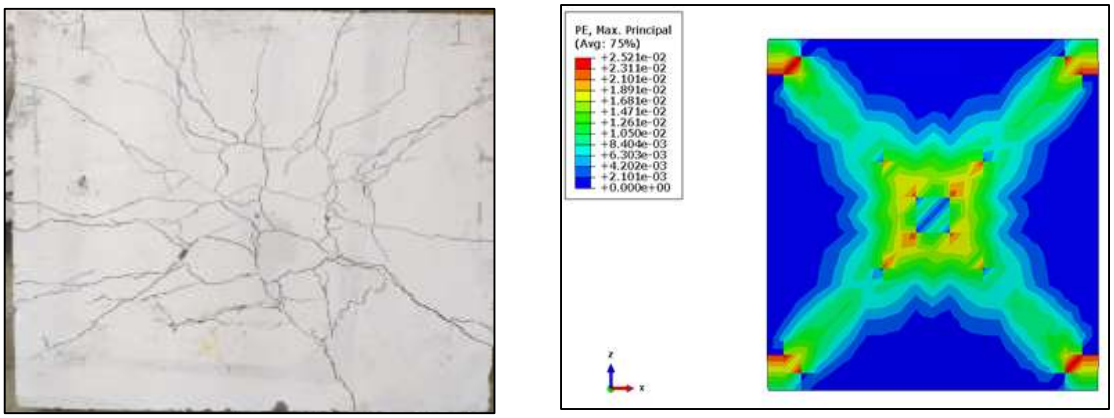

Figure 10. Cracking pattern on tension surface at ultimate monotonic load for specimens NRCP1.

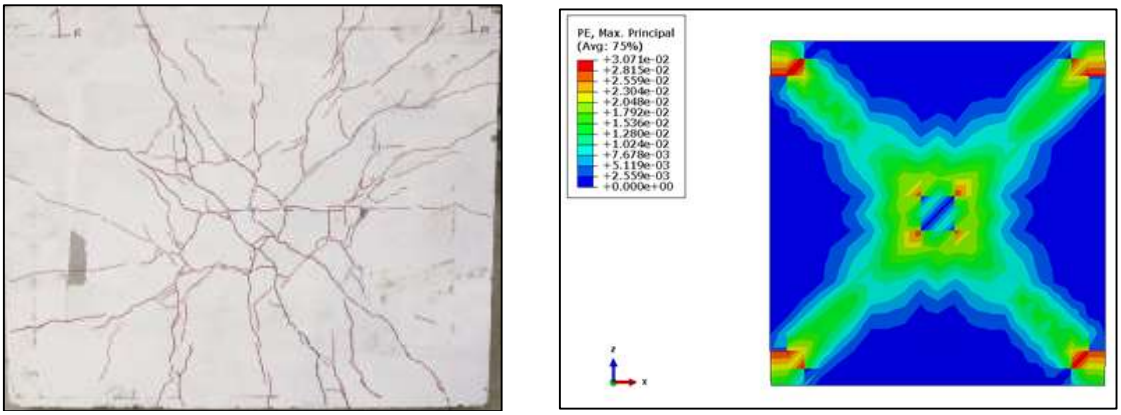

Figure 11. Cracking pattern on tension surface at ultimate repeated load for specimens NRCP2.

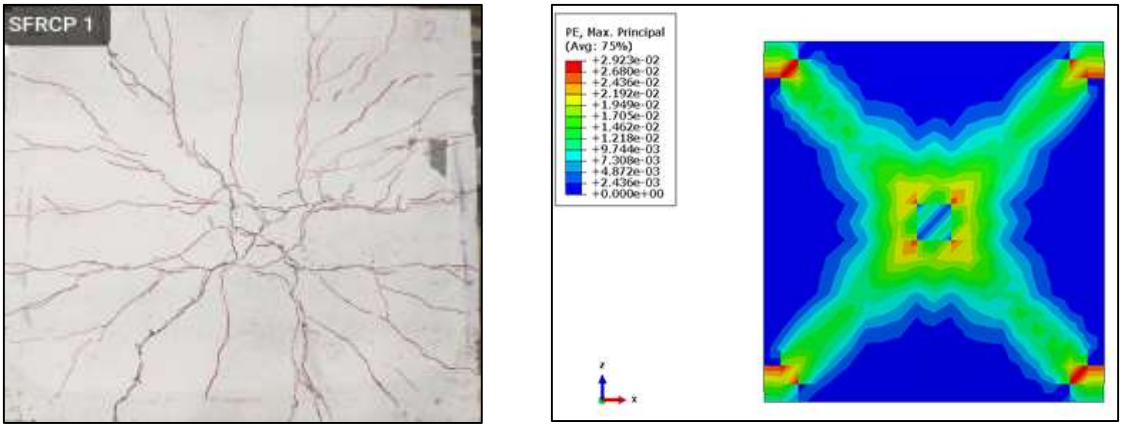

Figure 12. Cracking pattern on tension surface at ultimate monotonic load for specimen SFRCP1.

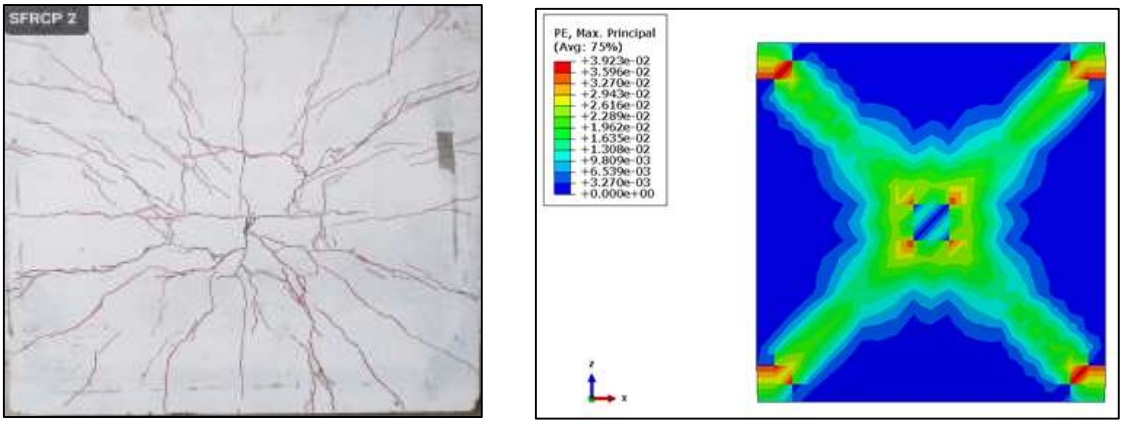

Figure 13. Cracking pattern on tension surface at ultimate repeated load for specimens SFRCP2.

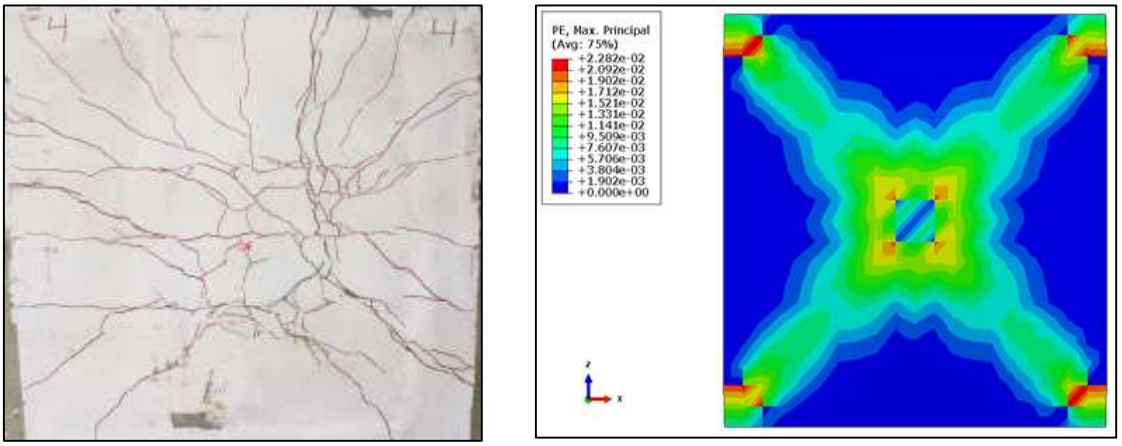

Figure 14. Cracking pattern on tension surface at ultimate monotonic load for specimens HFRCP1.

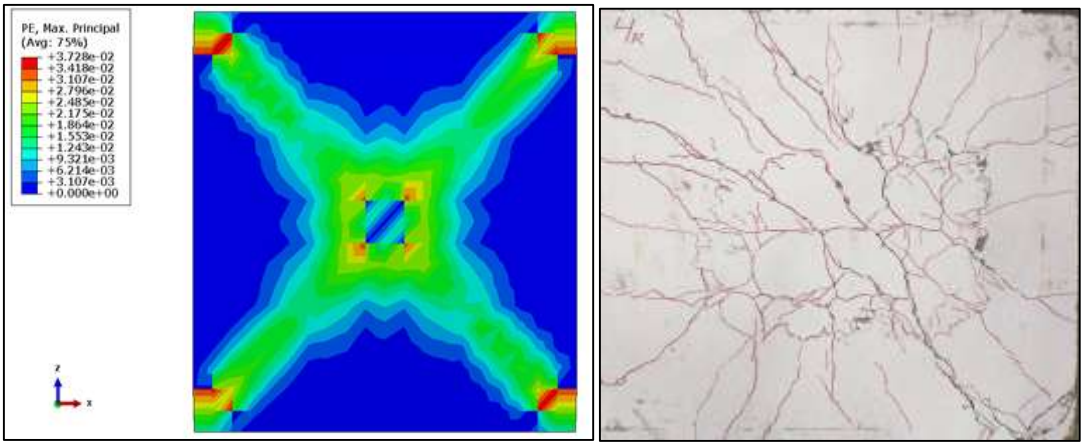

Figure 15. Cracking pattern on tension surface at ultimate repeated load for specimens HFRCP2.

5.3 Slab on soil model

The ABAQUS program simulates two types of concrete pavement specimens, assuming a layer of soil under the concrete pavement to simulate real pavement cases. These specimens are HFRCP1 and HFCP1. The slab on grade can be simulated using three-dimensional continuum solid elements. The model consists of a 120 mm concrete pavement layer placed on a virtual container having 6000mm ×6000mm side length and 3000 mm depth of subgrade soil. The properties of soil are detailed in **Table 8**. The soil is modeled as an elastic-plastic material with the Mohr-Coulomb yield criterion. The soil-concrete pavement interaction exhibits ‘‘tangential" and ‘‘normal" responses when the penalty type of formulation with a coefficient of 0.6 is used. The layer of soil is simulated with the same shape of concrete pavement to preserve the continuity of nodes between consecutive layers. The boundary conditions significantly impact predicting the model's response; the bottom surface of the subgrade and sides are assumed to be fixed.

Table 8. Soil data using presented Mohr-Coulomb model.

Material	Mass Density	Elastic Properties		Inelastic Properties			
Soil	1.44E-08	Young's Modulus MPa	Poisson 's Ratio	Friction Angle	Dilation Angle	Cohesion Yield Stress MPa	Absolute Plastic Strain
		150	0.3	41.5	11.5	0.001	0

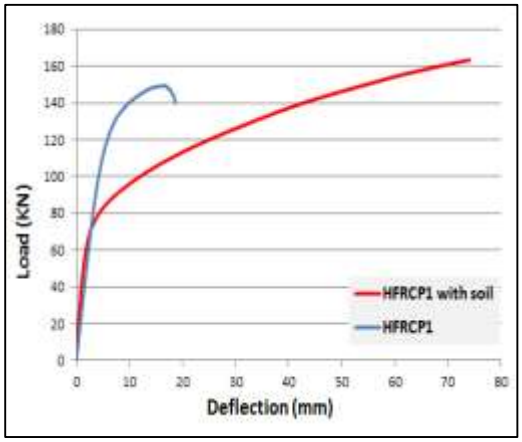

Figure 16. boundary condition of the model.

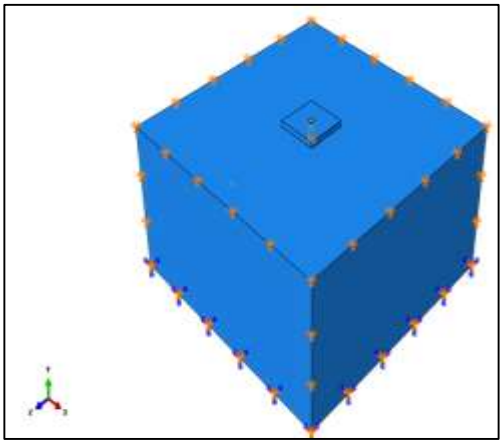

Figure 17. FEA load-deflection curves for HFRCP1 and HFRCP1 with soil under monotonic load.

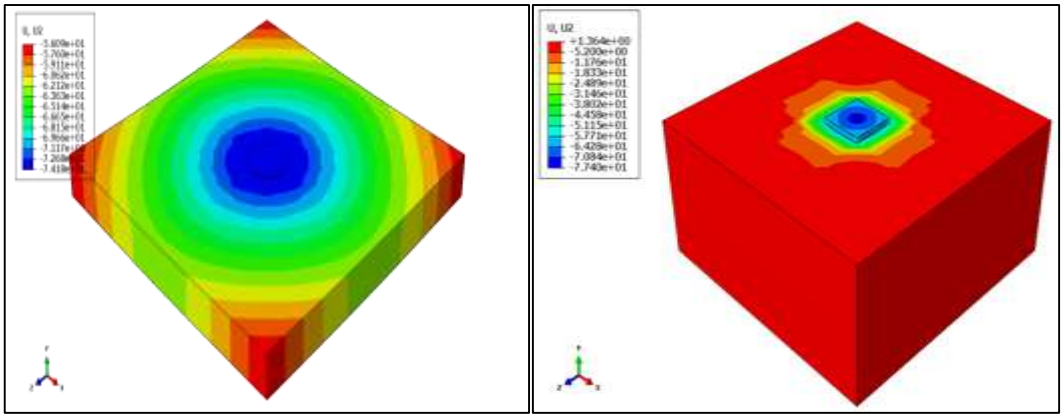

Figure 18. Vertical displacement along longitudinal direction of HFRCP1 with soil.

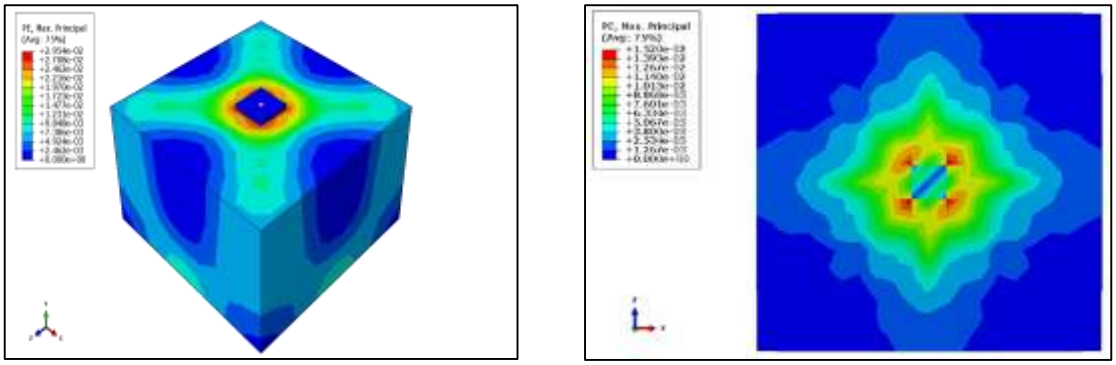

Figure 19. Cracking pattern on tension surface at ultimate monotonic load for specimen HFRCP1 with soil.

To study the behavior of fibrous hybrid pavements resting on soil, the HFCP1 specimen is selected. The specimen with the reinforcement steel bar completely replaced by hybrid fiber is chosen to test the fiber's contribution to flexural loading resistance and to verify the replacement of the main and secondary steel reinforcement in the concrete pavement for the real case when it is resting on the soil.

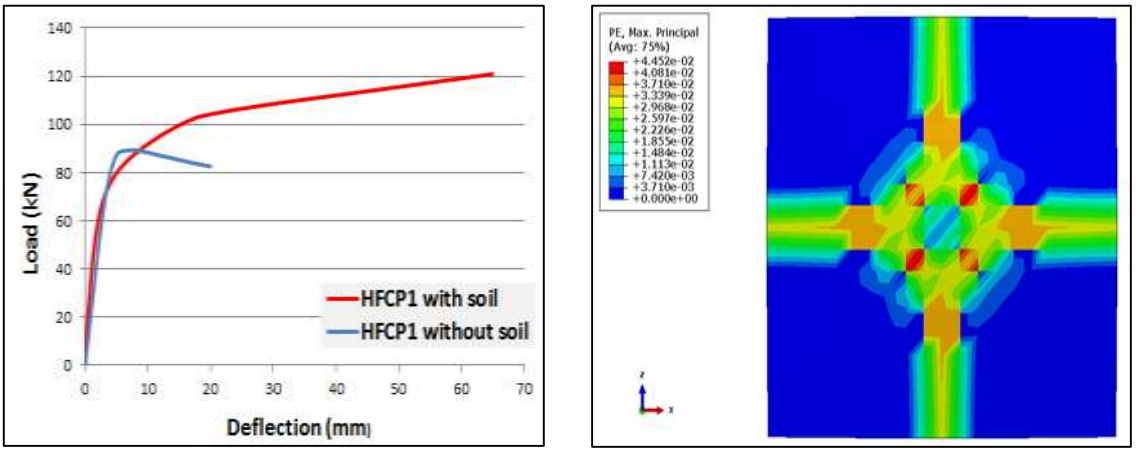

Figure 20. FEA load-deflection curves and cracking pattern on tension surface at ultimate monotonic load for specimens HFCP1 with soil.

6. PARAMETRIC STUDY

To study further parameters that may affect the rigid pavement response to the applied load, a parametric investigation is made considering the followings:

1. The fiber content in the concrete mix
2. The response of hybrid fiber reinforced concrete pavement without top reinforcement bars
3. The thickness of hybrid fiber reinforced concrete
4. The nature of loading, distributed, or concentrated

The specimens used in these cases are the hybrid fiber reinforced concrete pavement HFRCP (0.25% steel and 0.25% glass). This specimen is considered the optimum in the load resistance, ductility, and toughness of concrete. It is considered the best economic one.

6.1 Fiber Content

Fig.21 shows the applied load-displacement variation for the reinforced concrete pavement when the hybrid fiber ratio varies from 0.5% to 1%. The cracking contours are given in **Fig.22**.

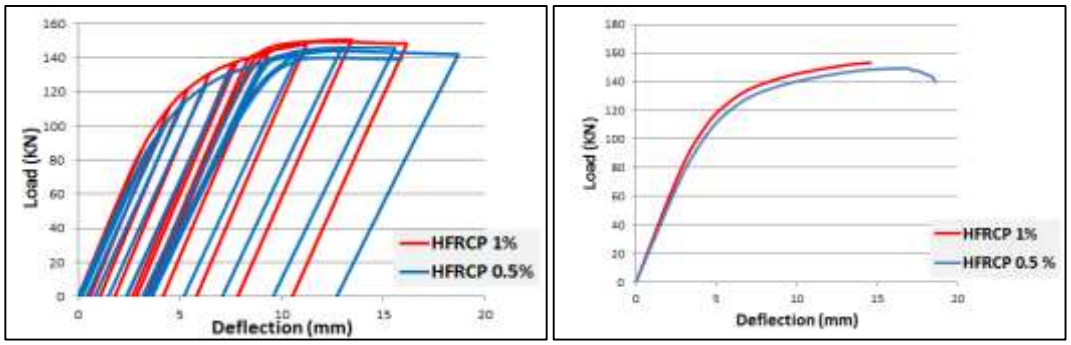

Figure 21 FEA load-deflection curves for specimens HFRCP 1% and HFRCP 0.5 % under monotonic and repeated load.

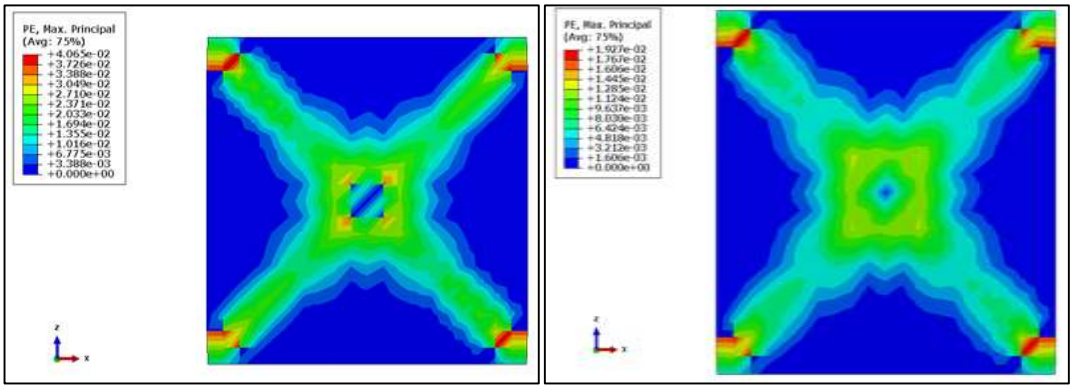

Figure 22. Cracking pattern on tension surface at ultimate monotonic and repeated load for HFRCP 1%.

6.2 Effect of top reinforcement

In this case, the top reinforcement existence in pavement HFPRCP (P: mean partially reinforced or without top reinforcement). The centrally applied load variation with central deflections and cracking contours are given in **Figs. 23 and 24**.

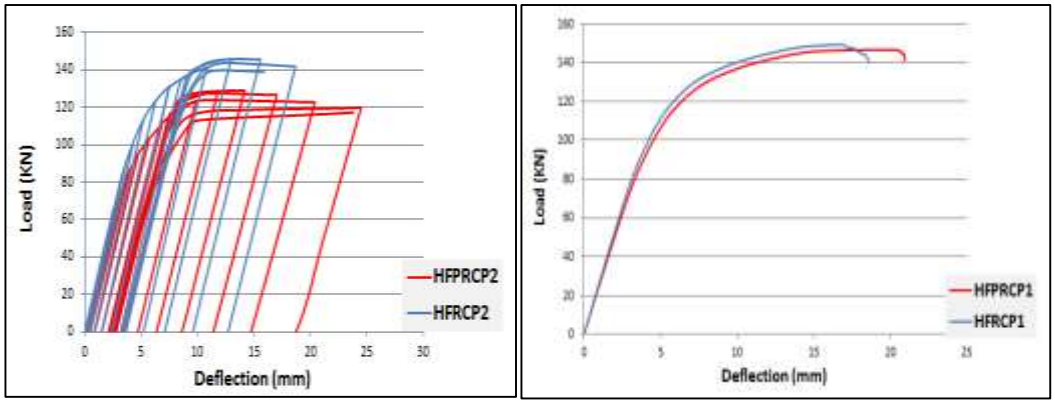

Figure 23. FEA load-deflection curves for specimen HFRCP and HFPRCP under monotonic and repeated load.

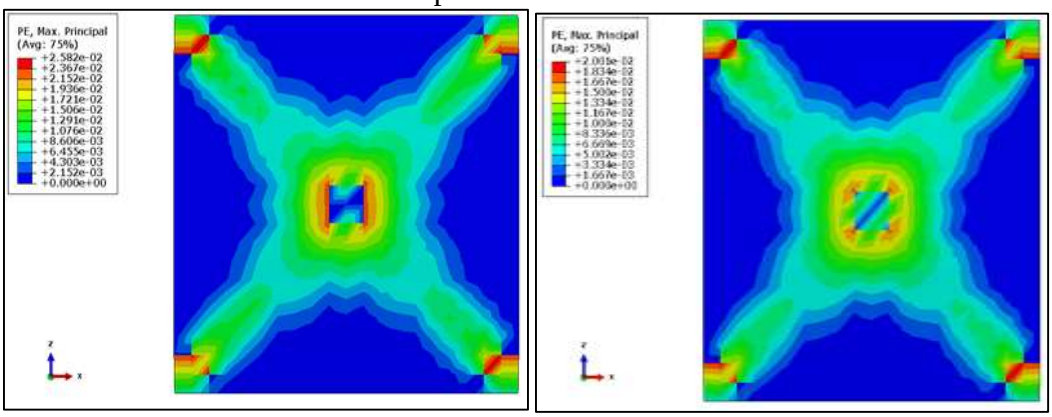

Figure 24. Cracking pattern on tension surface at ultimate monotonic and repeated load for specimens.

6.3 Pavement Thickness Effect

The hybrid fiber reinforced concrete (0.5% steel fiber and 0.5% glass fiber) thickness is varied to 180 mm. The selected bar diameter of reinforcement is 10 mm to obtain the same steel ratio for the 120 mm thickness pavement. The vertical displacement contours are given in **Fig.25**.

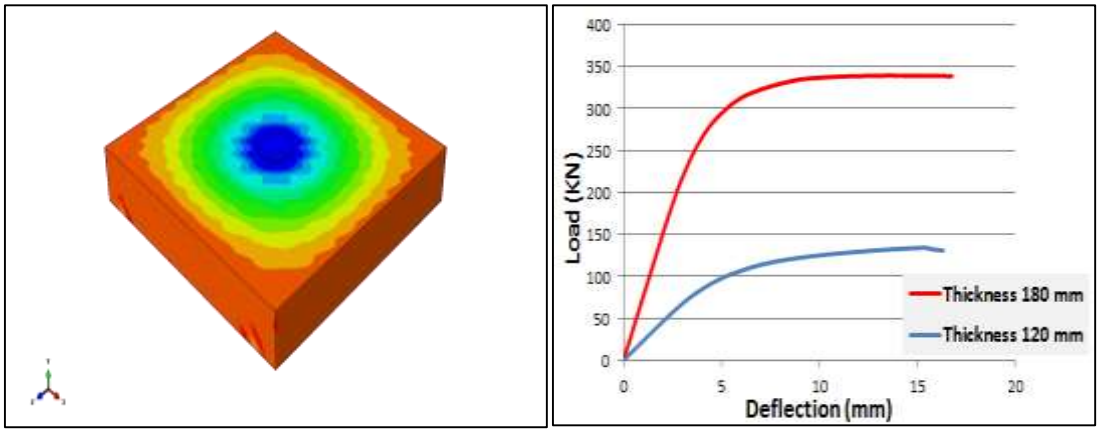

Figure 25. FEA load-deflection curves for specimens and Vertical displacement along longitudinal direction under monotonic load.

6.4 Effect of Distributed Load

The same HFRCP model is utilized to study the load type. When the concentrated load is distributed over the area of concrete pavement, the pavement shows a better load-displacement response is obtained as shown in **Fig.26** determined.

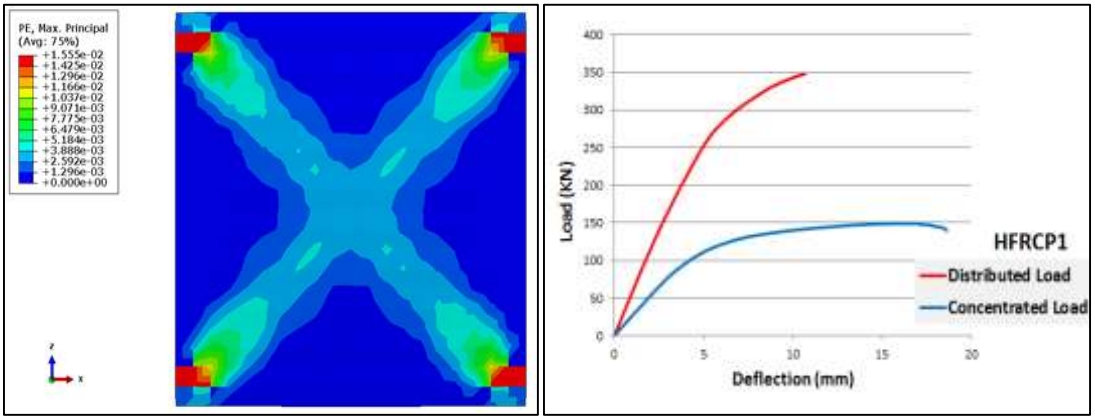

Figure 26. FEA load-deflection curves for specimen HFRCP1 and vertical displacement along longitudinal direction under monotonic distributed load.

7. CONCLUSIONS

1. The finite element model and the plasticity damage material models used in the present research can almost accurately predict the behavior of fiber-reinforced concrete pavement with and without soil under monotonic and repeated loading schemes. The numerical analyses show that the behavior of specimens and the ultimate loads are in good match with the experimental results for nonfibrous and fibrous reinforced concrete pavement.
2. The models implemented in the ABAQUS computer program can accurately predict the region of damage within the concrete pavement. The crack patterns obtained for the analyzed specimens using finite element models under monotonic and repeated loading are nearly identical to the crack patterns observed in the experimental work.
3. The numerical behavior of concrete pavement by the load-deflection curve under monotonic and repeated loading displays an acceptable agreement with the corresponding experimental curves.
4. The Mohr-Coulomb model is a simple linear elastic-perfect plastic model for geomaterials built into ABAQUS finite element software and is widely used in soil modeling to simulate the response of buried structures under monotonic loading. It was found that the specimen of hybrid fiber reinforced concrete pavement with 0.5% fiber content supported by the soil (the real pavement condition) may bear a greater load than the slab with simply-supported edges (pavement with leaching soil).
5. The load-deflection curves of hybrid fiber reinforced concrete pavement with 0.5 and 1% fiber show a slight difference in the behavior. This is due to the slight increase in the steel fiber content (0.25%) which has a major effect in increasing the properties of concrete as in pavement it is not economical to use higher percentages of fiber.
6. The load-deflection curves of hybrid fiber reinforced concrete pavement with 1% fiber reveal that the effect of the top layer reinforcement is very small on the bearing capacity

of the pavement in the case of the monotonic load. This is maybe due to bottom reinforcement adequacy in resisting bending moment resulting from applied loads. The slab thickness was adequate in resisting shear forces.

7. It has been found that when the thickness of the concrete pavement increases, keeping the steel ratio constant, the concrete becomes more rigid and withstands higher loads subjected to it.
8. It was found that the concrete pavement in the case of distributed load bears a higher load than the concentrated load state due to the spreading of the load over a larger area.

REFERENCES

- ABAQUS, 2012. Theory Manual, User Manual and Example Manual. Version 6.12, Providence, RI.
- ACI Committee 318, 2019, American Concrete Institute, & International Organization for Standardization. 2014. "Building code requirements for structural concrete (ACI 318M-19) and commentary", American Concrete Institute.
- AGENCY, F. E. M., 2007. Interim Testing Protocols for Determining the Seismic Performance Characteristics of Structural and Nonstructural Components. Federal Emergency Management Agency Washington, DC
- Belletti, B. and Cerioni, R. Meda, A., and Plizzari, G. A., 2004. Experimental and numerical
- analyses of FRC slabs on grade, In Proceedings of FRAMCOS5 Conference, Vail Colorado: 973-980.
- British Standards Institution, 2004. Eurocode 2 "Design of Concrete Structures: Part 1-1: General Rules and Rules for Buildings", British Standards Institution
- Daniel, J. I. et al., 2002. Report on Fiber Reinforced Concrete Reported by ACI Committee 544, 96 (Reapproved).
- Ergatoudis, I., Irons, B. M., and Zienkiewicz, O. C., 1968. Curved, isoparametric, quadrilateral elements for finite element analysis, *International Journal of Solids and Structures*, 4(1), pp. 31–42.

- Khan, M. I., and Harwalkar, A. B., 2014. Mechanistic analysis of rigid pavement for wheel load stresses using Ansys, International Journal of Research in Chemistry and Environment, 4(1): 79–90.
- Kwak, H.-G., and Filippou, F. C., 1990. Finite element analysis of reinforced concrete structures under monotonic loads. Department of Civil Engineering, University of California Berkeley, CA.

- Lundqvist, J., 2007. Numerical Analysis of Concrete Elements Strengthened With Carbon Fiber Reinforced Polymers. (Doctoral dissertation, Luleå Tekniska Universitet).

- Shakir, H., 2021. Behavior of Fiber Reinforced Concrete Pavement under Dynamic Loading. Master's Thesis. Al-Nahrain University.

- Zimmer, J., Klein, D., and Stommel, M., 2015. Experimental And Numerical Analysis Of Liquid-Forming, Key Engineering Materials, 651–653(06): 842–847.